Proceedings of Equadiff-11
2005, pp. 17–26
ISBN 978-80-227-2624-5

ON AB-INITIO COMPUTATIONS FOR PHASE CHANGE PROBLEMS IN SOLIDS

THOMAS BLESGEN*

Abstract. At the example of a particular segregation problem from mineralogy, quantitative simulations based on ab-initio methods are done. Using in particular the harmonic approximation, the free energy of the physical process for a range of concentration vectors is calculated as well as diffusion and elasticity coefficients. The obtained data are the foundations of high-precision finite element computations. For selected configurations, the computed free energies are validated with results from quantum mechanics.

Key words. ab-initio computations, multi-scale problems, quantum mechanics

AMS subject classifications. 35K55, 65M60, 74N99

1. Introduction. The present work is concerned with computer simulations of the so-called chalcopyrite disease within sphalerite. This is a well-known and extensively-discussed problem arising in geology. The quantitative description of this process helps to get a precise understanding of the time scales involved in magma ascending from earth's core and might lead to better predictions for earth quakes and volcano eruptions. The study of this problem is an example to illustrate how one can successfully bridge different length scales and do simulations closer to experiment.

Characteristic for chalcopyrite disease is the presence of a melon-type structure close to the boundary of a rock sample.

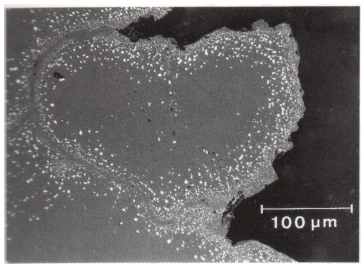

FIG. 1.1. *Part of the boundary region of a rock sample with chalcopyrite disease (reflecting light image), black matrix: sphalerite, white grains: chalcopyrite.*

The common understanding is that these structures develop during a long time period in the range of several hundred thousand years. Since no experimentalist would be so patient, mineralogists studied chalcopyrite disease under altered conditions in the laboratory, where they surround a ZnS single crystal by sulphur gas, spread copper powder at its surface, and significantly increase temperature (kept isothermally between $T = 550°\mathrm{C}$ and $T = 700°\mathrm{C}$), see the reports of the experiments [2], [3]. By the increase of T (and sufficiently high sulphur fugacity) the process is accelerated and the characteristic pattern formation is observed after several weeks ($T = 700°$) or months ($T = 550°$).

*Max-Planck-Institute for Mathematics in the Sciences, Inselstraße 22-26, D-04103 Leipzig, Germany (blesgen@mis.mpg.de).

Chalcopyrite disease is caused by gradients of the chemical potential induced by an increase of external sulphur fugacity. Hereby, the primary Fe^{2+} is oxidised to Fe^{3+} and reacts with copper diffusing into the Fe-containing sphalerite crystal to chalcopyrite ($= CuFeS_2$). During the process, gas S^{2-} molecules attach to the crystal surface. Since roughly speaking the formation of chalcopyrite phases can only take place after a sufficient amount of Cu has diffused into the matrix, the generic mechanism has been called *diffusion induced segregation* or shortly DIS.

The mathematical analysis of chalcopyrite disease presented in this work is based on partial differential equations and a thermodynamical description and tries to understand the physics underlying these examinations with the goal to make simulations close to the ideal experimental conditions. The developed model represents chalcopyrite disease on a medium spatial scale, the microstructure is not resolved. The main idea persued in this article is to insert expressions of the free energy gained from ab initio calculations into (standard) finite element computations.

2. Mathematical formulation. Let Ω be a (time-independent) domain in $\mathbb{R}^D$, $1 \leq D \leq 3$ containing the crystal. By $0 < T_0 < \infty$ we denote a stop time and by $\Omega_T := \Omega \times (0, T_0)$ a cylinder in space-time. $c_i = c_i(x,t)$ denotes the relative number of species i, $i \in \{1,2,3\}$ per available lattice point at time t and space point $x \in \Omega$, where we set

$$c_1 \approx \text{Fe}, \quad c_2 \approx \text{Cu}, \quad c_3 \approx \text{Zn}, \quad c_4 \approx \text{vacancies}.$$

c_1 satisfies $c_1 = \frac{N_{\text{Fe}}}{N_{\text{Me}}}$, where N_{Fe} is the number of Fe atoms and N_{Me} the number of metal ion sites. Similar relationships hold for c_2 and c_3. We will not model the attachment of S molecules at the lattice surface and assume that the concentration of S is identically $c_S := 0.5$. Due to electric neutrality we postulate, see [2], [4],

$$c_4 = \frac{1}{2} c_1. \tag{2.1}$$

By mass conservation the concentration vector c thus fulfills

$$c = (c_1, c_2, c_3) \in \Sigma := \Big\{ (\tilde{c}_1, \tilde{c}_2, \tilde{c}_3) \in \mathbb{R}^3 \,\Big|\, \tilde{c}_i \geq 0,\ \frac{3}{2}\tilde{c}_1 + \tilde{c}_2 + \tilde{c}_3 \equiv \frac{1}{2} \Big\}.$$

The constitutive relation for the mass fluxes is assumed to be of the isotropic Onsager form, [15],

$$J_i = \sum_{j=1}^{3} L_{ij} \nabla \mu_j, \quad 1 \leq i \leq 3. \tag{2.2}$$

L, the mobility, is symmetric due to Onsager's reciprocity law and a positive semi-definite 3×3 tensor. Furthermore,

$$\mu_j = \frac{\partial f}{\partial c_j}$$

is the chemical potential. To simplify the existence theory we assume that L is positive definite. The total Helmholtz free energy density f consists of f_1 for chalcopyrite and f_2 for sphalerite. Hence, the two different phases or lattice orders are characterised by two different free energies, and f is the convex hull of f_1 and f_2.

The characterisation of the phases is given within the framework of functions of bounded variation $BV(\Omega)$. It is convenient to introduce the set

$$V := \{\tilde{\chi} \in BV(\Omega) \mid \tilde{\chi}(1-\tilde{\chi}) = 0 \text{ a.e. in } \Omega\} \tag{2.3}$$

and choose for the free energy with a constant $\gamma > 0$ the convex-combination

$$F(c,\tilde{\chi}) := \int_\Omega \gamma|\nabla\tilde{\chi}| + \int_\Omega (\tilde{\chi} f^1(c) + (1-\tilde{\chi}) f^2(c)). \tag{2.4}$$

The first integral $\int_\Omega \gamma|\nabla\tilde{\chi}|$ defines the (constant) surface energy.

To conclude, we are concerned with the formulation

Find the vector $c = (c_1, c_2, c_3)$ and χ such that in $\Omega \subset \mathbb{R}^D$ for $t > 0$

$$\partial_t c_i = \operatorname{div}\Big(\sum_{j=1}^{3} L_{ij}\nabla\mu_j\Big), \quad i = 1,2,3, \tag{2.5}$$

$$\mu_i = \chi\frac{\partial f^1}{\partial c_i}(c) + (1-\chi)\frac{\partial f^2}{\partial c_i}(c), \quad i = 1,2,3, \tag{2.6}$$

$$F(c,\chi) = \min_{\tilde{\chi}\in V} F(c,\tilde{\chi}) \tag{2.7}$$

with the initial and boundary conditions

$$c_i(x,0) = c_{0i}(x),\ i = 1,2,3; \qquad \chi(x,0) = \chi_0(x) \quad \text{in } \Omega, \tag{2.8}$$

$$\left.\begin{aligned} \partial_\nu\chi &= 0, \\ c_i &= g_i, \quad 1 \le i \le 3 \\ \mu_i &= h_i, \quad 1 \le i \le 3 \end{aligned}\right\} \qquad \text{at } \partial\Omega. \tag{2.9}$$

We stress that (2.7) actually means that the free energy is in a *global* minimum with respect to χ. For most physical systems, this assumption is not reasonable. But here, the segregation dramatically changes the local lattice order such that there is a huge start energy and at least approximately a global minimum is obtained. If we replace (2.7) by an Allen-Cahn equation, the system may get stuck in a local minimum and flipping over from sphalerite to chalcopyrite may become impossible at large times t, see the detailed discussion in [6].

The following theorem is covered by the results in [5]. It is formulated for classical Dirichlet boundary conditions $g_i = h_i = 0$ when (2.7) is replaced by a parabolic equation.

THEOREM 2.1 (Global existence of solutions for System (2.5)–(2.9)).
There exists a weak solution (c,μ,χ) of (2.5)–(2.9) such that

(i) $c \in C^{0,\frac{1}{4}}([0,T_0];\, L^2(\Omega;\mathbb{R}^3))$,

(ii) $\partial_t c \in L^2(0,T_0;\, (H_0^1(\Omega;\mathbb{R}^3))')$,

(iii) $\mu \in L^2(0,T_0;\, H_0^1(\Omega;\mathbb{R}^3))$,

(iv) $\chi \in L^2(0,T_0;\, BV(\Omega))$ *with* $\chi(1-\chi) = 0$ *almost everywhere in* Ω.

In general the solution (c,μ,χ) is not unique since χ may not be unique.

3. General outline of the numerical solution ansatz. We solve the weak formulation of (2.5)–(2.9) with linear finite elements. The arising discrete system is solved

with a Newton-Krylov method. This is a Quasi-Newton scheme where the inner linear loop is solved with the generalized minimal residual method, GMRES. This combines the fast convergence of Newton's method with the excellent damping properties of GMRES.

The various possibilities to speed up the finite element code like parallelisation by multi-grid methods or domain decomposition are not exploited. In order to incorporate approximations of the physical free energy, we will persue the following ansatz. Let c be a given concentration vector. In a first independent computation step two approximations $f^1(c)$ and $f^2(c)$ are computed that simulate the actual free energy density of the material in the bulk phases, hence represent two local minima of f. The main computational tool is the *harmonic approximation* with GULP, [9], and the values $f^1(c)$, $f^2(c)$ are obtained from modified chalcopyrite and sphalerite configurations. Furthermore we apply molecular dynamics (MD) simulations with DLPOLY, `http://www.cse.clrc.ac.uk/msi/software/DL_POLY/`. For quantum mechanical (QM) computations we use ABINIT, [10], (`http://www.abinit.org`).

Generally, $f^1(c)$ and $f^2(c)$ are stored beforehand in huge data bases. Each entry in these data bases references to a small range of concentration vectors c (approximation of f^l by piecewise constant functions).

It remains to find approximations for $\frac{\partial f^m}{\partial c_j}$. This is done by central differencing of the tabular entries where possible and by one sided differences at the beginning and end of the data base. To make this precise, let $M_j \in \mathbb{N}$ be the dimension of the data base w.r.t. c_j, that is $f^m(c_1, \ldots, c_j, \ldots, c_3)$ is constant for $c_j \in [c_j^l, c_j^{l+1})$, $1 \le l \le M_j - 1$. Set for $c_j \in (c_j^l, c_j^{l+1})$ (suppressing frozen components c_α for $\alpha \neq j$)

$$\frac{\partial f^m}{\partial c_j}(c_j) := \begin{cases} \dfrac{f^m(c_j^{l+1}) - f^m(c_j^{l-1})}{c_j^{l+1} - c_j^{l-1}} & \text{if } 2 \le l \le M_j - 1, \\ \dfrac{f^m(c_j^1) - f^m(c_j^2)}{c_j^1 - c_j^2} & \text{if } l = 1, \\ \dfrac{f^m(c_j^{M_j}) - f^m(c_j^{M_j-1})}{c_j^{M_j} - c_j^{M_j-1}} & \text{if } l = M_j. \end{cases} \tag{3.1}$$

After numerical tests with analytic expressions for f, the parameters $M_1 = M_3 = 30$, $M_2 = 40$ were chosen. Larger values of M_j are desirable as they reduce the approximation errors but the computations become too costly.

4. Free energy computation with GULP. The theory of the harmonic approximation is explained in [1], [8]. For the computations within GULP we have to fit the heuristic potentials that represent the short-range interatomic potentials. We begin with ZnS. We use the *Buckingham potential*

$$\phi(r) := -4\varepsilon \left(\frac{\sigma}{r}\right)^6 + B \exp\left(\frac{-r}{\rho}\right) \tag{4.1}$$

that gives in practise better results than Lennard-Jones potentials. In (4.1), r is the interatomic distance, σ that particular interatomic distance where the energy vanishes and ε is the potential energy at equilibrium separation. The term $(\frac{\sigma}{r})^6$ describes the van-der Waals induced dipole moments whereas the exponential stands for the repulsive forces.

We use a shell model where the rigid atom is split into an inner part comprising of the nucleus with the tightly bound inner electrons and into an outer part with the loosely

		Exp1	Exp2	P1	P2	P3
a	[Å]	5.41	5.41	5.403	5.403	5.402
V	[Å^3]	158.29	158.29	157.77	157.77	157.69
C_{11}	[GPa]	9.42	9.76	8.6	9.37	9.18
C_{12}	[GPa]	5.68	5.9	6.54	6.16	5.83
C_{44}	[GPa]	4.36	4.51	3.8	4.03	4.41
$\varepsilon_{\text{stat}}$		7.9	–	8.565	7.21	7.33
ε_{hf}		5.8	–	4.815	4.56	3.64

Table 4.1
Comparison of experimental and calculated data for ZnS.

		P1	P2	P3
Potential Parameters:				
$\underline{S\text{-}S}$				
A	[eV]	1200.0	1200.0	1200.0
ρ	[Å]	0.149	0.149	0.149
B	[eV Å^6]	120.0	120.0	120.0
$\underline{\text{Zn-}S}$				
A	[eV]	613.36	613.36	528.9
ρ	[Å]	0.399	0.399	0.411
B	[eV Å^6]	0.0	0.0	0.0
Shell Model:				
SK_S	[eVÅ^{-2}]	12.7	12.7	16.86
Zn K_S	[eVÅ^{-2}]	0.0	0.0	2.181
Three Body Terms:				
S-Zn-S force constant	[eV rad^{-2}]		0.713	0.713
S-Zn-S bond angle	[degrees]		109.47	109.47
k_2	[eV rad^{-2}]		3.0	3.0
k_3	[eV rad^{-3}]		3.0	3.0
k_4	[eV rad^{-4}]		5.0	5.0

Table 4.2
Potential parameters for P1, P2 and P3 used for ZnS.

bound shell electrons. This allows to take dipole moments into account. Additionally, a harmonic three-body potential is used to account for the directionality on the S-Zn-S bond according to the Taylor expansion

$$W_{3b}(\theta) := \frac{1}{2}k_2(\theta-\theta_0)^2 + \frac{1}{6}k_3(\theta-\theta_0)^3 + \frac{1}{12}k_4(\theta-\theta_0)^4,$$

where θ_0 is the angle of the unstressed three-body system and k_2, k_3 and k_4 determine the sensibility w.r.t. angular changes.

GULP sets up interactions of potentials between shells and other atoms/shells and these potentials must be fitted to give reasonable results. For sphalerite and chalcopyrite this is a tricky business, probably because the bondings in sulphides are not purely ionic but may range from ionic to covalent through to metallic. A least squares fit to measured parameters is carried out, Table 4.1.

Here, a is the lattice parameter of the cubic lattice, V is the volume of the unit cell, C_{il} are the elastic constants. To find the potential parameters, one starts with a simple model without shells where the charges of S and Zn are fixed to -2 and $+2$. By a least squares optimisation run the parameters for the spring constant and in case of sphalerite for the $\mathrm{S}-\mathrm{Zn}-\mathrm{S}$ interactions are fitted. The parameters thus obtained are then used in

		Exp2/QM	P4	P5
a	[Å]	5.2864	5.601	5.59
b	[Å]	5.2864	5.601	5.59
c	[Å]	10.4102	10.71	10.70
V	[Å^3]	145.46	168.08	167.73
C_{11}	[GPa]	*17.83*	18.02	18.12
C_{12}	[GPa]	*5.81*	5.67	5.64
C_{13}	[GPa]	*6.27*	6.59	6.59
C_{33}	[GPa]	*13.15*	14.23	14.25
C_{44}	[GPa]	*13.19*	18.86	18.93
C_{66}	[GPa]	*4.93*	8.68	8.70

Table 4.3
Experimental/quantum mechanical and calculated data for chalcopyrite.

		P4	P5
Potential Parameters:			
<u>S-S</u>			
A	[eV]	1200.0	1200.0
ρ	[Å]	0.508	0.508
B	[eV Å^6]	120.0	120.0
<u>Fe-S</u>			
A	[eV]	5694.68	5694.68
ρ	[Å]	0.2748	0.2748
B	[eV Å^6]	0.0	0.0
<u>Cu-S</u>			
A	[eV]	110.62	100.619
ρ	[Å]	0.327	0.327
B	[eV Å^6]	0.0	0.0
Shell Model:			
SK_S	[eVÅ^{-2}]	12.70	12.70
Three Body Terms:			
S-Cu-S force constant	[eV rad^{-2}]		0.01164
S-Cu-S bond angle	[degrees]		109.47
k_2, k_3, k_4	[eVrad^{-2}]		2.5, 2.5, 4.0
S-Fe-S force constant	[eV rad^{-2}]		0.01169
S-Fe-S bond angle	[degrees]		109.47
k_2, k_3, k_4	[eVrad^{-2}]		2.5, 2.5, 4.0

Table 4.4
Potential parameters for P4 and P5 used for chalcopyrite.

an extended model that includes shells and three-body terms.

For P1, a Buckingham potential is fitted and a shell is only used for the S ions. In P2, a three-body potential for S-Zn-S is added. In particular this results in better values for C_{44}, $\varepsilon_{\mathrm{hf}}$ and $\varepsilon_{\mathrm{st}}$. In P3 a shell to the Zn is included, see Table 4.2.

The data set EXP1 refers to the experimental results in [14], EXP2 to the recently made measurements (where $\varepsilon_{\mathrm{stat}}$ and $\varepsilon_{\mathrm{hf}}$ were not measured).

The agreement documented in Table 4.1 is suitably well with an error in the size of uncertainty of the measured parameters. P2 and P3 seem both be very well suited to represent the structure of ZnS.

The fitting procedure to chalcopyrite is similar. For P4, Cu and Fe cores replace Zn. The S shell is fitted to yield good values for the lattice constants and the volume of the primitive cell. But there is one bottleneck: up to now it has not been possible to measure the elastic parameters C_{il} for chalcopyrite in experiment. The slanted parameters in

TABLE 4.3 are the result of the quantum mechanical computations in Section 5 and the GULP potential is fitted to these parameters. To further improve the quality of the results, three-body potentials for S-Cu-S and S-Fe-S are added. TABLE 4.3 provides the results of the fitting, TABLE 4.4 the fitting parameters. We see that there is almost no improvement by using the three-body potentials. The agreement to the quantum mechanical parameters is good, except for C_{44} and C_{66}.

5. Quantum mechanical computations. We perform quantum mechanical computations using ABINIT, [10]. The Born-Oppenheimer approximation of the Schrödinger equation is solved with the local-density approximation within the framework of density function theory, [11], [12], [16]. For the representation of the electron-atom-interactions Troullier-Martins pseudopotentials, [17], are used.

After simple convergence tests, the energy cutoff e_{cut} was set to $20Ha \approx 544.23\,\text{eV}$ (one has $e_{\text{cut}} = \frac{1}{2}[2\pi(k + G_{\max})]^2$, and $G_{\max}$ is the largest reciprocal lattice vector included in the Bloch-Expansion of the wave function) yielding a relative error of 0.4% in the total energy. The macroscopic dielectric constant $\varepsilon_{\text{diel}}$ of ZnS is preset to 8.32, the physical value found in literature. For the self-consistent energy minimisation cycle within ABINIT, the conjugated gradient method is chosen. In order to obtain satisfying results, the Brillouin zone is sampled with 182 k-points.

The minimal value $-7.22\,\text{eV}$ is obtained at $a = 5.317\text{Å}$ (the binding energy computed by GULP for $a = 5.419$ is $-7.676\,\text{eV}$). A slight underestimate of the lattice constant and an overestimate of the binding energy are typical of well-converged local-density calculations.

The computations for chalcopyrite are similar to those of ZnS. After convergence studies the energy cutoff e_{cut} was set to $30Ha \approx 816.35\,\text{eV}$ resulting in a relative error of 0.3%. Unfortunately, $\varepsilon_{\text{diel}}$ is unknown for chalcopyrite, so that for the first computations of the relaxed geometry the ZnS-value is taken for chalcopyrite, too. Numerical tests have shown the results for chalcopyrite to change by less than 0.1% for different values of $\varepsilon_{\text{diel}}$. As in the case of sphalerite the Brillouin zone was sampled with 182 k-points. A not too small value is essential for the quality of the results.

The minimal binding energy for chalcopyrite is $-19.7\,\text{eV}$ and obtained at $a = b = 5.061\text{Å}$, $c = 9.969\text{Å}$. The binding energy computed by GULP is $-20.57\,\text{eV}$.

In the remainder of this section we compute C_{ij} via the acoustical modes. The obtained elastic constants are needed to gauge the interatomic potentials within GULP. The elastic constants for sphalerite serve as comparison and validation of the method.

Travelling waves in crystals (as waves in general) can be represented by

$$u(r,t) = \tilde{u}\exp(i(k \cdot r - \omega t)). \tag{5.1}$$

Here, u is the atomic elongation, $\tilde{u} = (\tilde{u}_1, \tilde{u}_2, \tilde{u}_3)$ is the amplitude vector, $k = (k_1, k_2, k_3)$ the wave vector, $r = (r_1, r_2, r_3)$ the position vector and ω the angular frequency. The strain ε is given by

$$\varepsilon_{ij} = \frac{1}{2}\Big(\frac{\partial u_i}{\partial x_j} + \frac{\partial u_j}{\partial x_i}\Big). \tag{5.2}$$

With ABINIT we compute *dispersion curves*, i.e. curves that describe the relationship $k \mapsto \omega(k)$. More precisely we estimate with interpolation formulas the slopes $\omega'(0)$ of the acoustic phonon dispersion curves at the origin (acoustic phonon modes in contrast to optical phonon modes fulfill $\omega(k = 0) = 0$). Using (5.1) in (5.2) yields

$$\varepsilon_{lj}(t) = \frac{i}{2}\Big(u_l(t)k_j + u_j(t)k_l\Big) = \frac{i}{2}\Big(\tilde{u}_l k_j + \tilde{u}_j k_l\Big)\exp(i(k \cdot r - \omega t)).$$

From Newton's equation of motion $\rho\partial_t^2 u_n = -\rho\omega^2 u_n$ we get

$$\rho\omega^2 \tilde{u}_n = \sum_{jlm} C_{njlm} k_j k_l \tilde{u}_m \qquad \text{or} \qquad \rho\omega^2 \tilde{u} = M(k)\cdot\tilde{u}.$$

		Exp1	Exp2	QM	P2
a	[Å]	5.41	5.41	5.32	5.403
V	[Å^3]	158.29	158.29	150.36	157.77
B_0	[GPa]	76.6	–	82.8	71.55
C_{11}	[GPa]	9.42	9.76	9.63	9.37
C_{12}	[GPa]	5.68	5.9	5.89	6.16
C_{44}	[GPa]	4.36	4.51	4.87	4.03
$\varepsilon_{\text{stat}}$		7.9	–	–	7.21
ε_{hf}		5.8	–	–	4.56

Table 5.1
Comparison of experimental and calculated data for ZnS.

		Exp2	QM	P5
a	[Å]	5.2864	5.061	5.59
b	[Å]	5.2864	5.061	5.59
c	[AA]	10.4102	9.969	10.70
V	[Å^3]	145.46	127.67	167.73
C_{11}	[GPa]	–	17.83	18.12
C_{12}	[GPa]	–	5.81	5.64
C_{13}	[GPa]	–	6.27	6.59
C_{33}	[GPa]	–	13.15	14.25
C_{44}	[GPa]	–	13.19	18.93
C_{66}	[GPa]	–	4.93	8.70

Table 5.2
Comparison of experimental/calculated data for chalcopyrite.

The values on the left hand side are provided by ABINIT. Suitable k-points can be gained by densifying the k-point mesh (with `dsifkpt`). It remains to compute the matrix M which is straightforward using the Voigt notation. For ZnS we find

$$M(k) = \begin{pmatrix} C_{11}k_1^2 + C_{44}(k_2^2+k_3^2) & (C_{12}+C_{44})k_1k_2 & (C_{12}+C_{44})k_1k_3 \\ (C_{12}+C_{44})k_1k_2 & C_{11}k_2^2 + C_{44}(k_1^2+k_3^2) & (C_{12}+C_{44})k_2k_3 \\ (C_{12}+C_{44})k_1k_3 & (C_{12}+C_{44})k_2k_3 & C_{11}k_3^2 + C_{44}(k_1^2+k_2^2) \end{pmatrix}$$

and for tetragonal chalcopyrite it holds

$$M(k) = \begin{pmatrix} C_{11}k_1^2 + C_{66}k_2^2 + C_{44}k_3^2 & (C_{12}+C_{66})k_1k_2 & (C_{13}+C_{44})k_1k_3 \\ (C_{12}+C_{66})k_1k_2 & C_{66}k_1^2 + C_{11}k_2^2 + C_{44}k_3^2 & C_{44}k_2k_3 \\ (C_{13}+C_{44})k_1k_3 & C_{44}k_2k_3 & C_{44}(k_1^2+k_2^2) + C_{33}k_3^2 \end{pmatrix}.$$

Table 5.1 below shows the results of the computations for ZnS and extends the results of Table 4.1. EXP1 and EXP2 are as before, PS2 refers to GULP results, QM to quantum mechanical data. B_0 denotes the bulk modulus.

Table 5.2 lists the results for chalcopyrite. The computed lattice constants are about 6% off the experimental values. Probably, the Troullier-Martins pseudopotentials are too soft.

6. Numerical results. Now we will focus on numerical solutions to System (2.5)–(2.9) in its dimensional form in 2D based on the tabulated free energy and linear finite elements. FIG. 6.1 shows the results of a finite element computation based on the tabulated harmonic free energy.
Physical Parameters: $\Omega = [0, 0.2\text{m}] \times [0, 0.1\text{m}]$, $T = 500°C$, $\gamma = 3 \cdot 10^{-9} m$, $D_{\text{Cu}} = D\text{Cu}(c) \approx 2.6 \cdot 10^{-4} m^2/s$, dependence on c computed by Green-Kubo relations, $D_{\text{Fe}} \equiv 1.26 \cdot 10^{-4} m^2/s$, $D_{\text{Zn}} \equiv 1.85 \cdot 10^{-7} m^2/s$.
Triangulation Data: 33153 points, 65536 triangles, $h = 10^{-8}$.
General Parameters: $\epsilon_{\text{GMRES}} = \triangle t = 0.004$, $\eta = 10^{-8}$.
Initial Conditions: $c_{10} \equiv 0.066$, $c_{20} \equiv 0.001$ in Ω, χ_0 minimum of $\chi \mapsto F(c_0, \chi)$.
Boundary conditions: $\partial_\nu c_1 = \partial_\nu c_3 = \partial_\nu \chi = 0$ and $c_2 = 0.25$ on $\partial\Omega$.

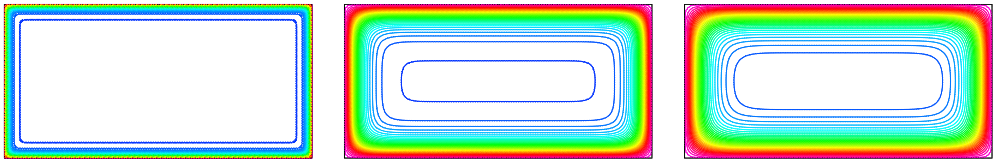

FIG. 6.1. *Diffusion of Cu. The density of the level sets indicates the steepness of the copper gradient. At $t = 0$, the initial datum falls from 0.25 at $\partial\Omega$ to 0.001 in Ω.*

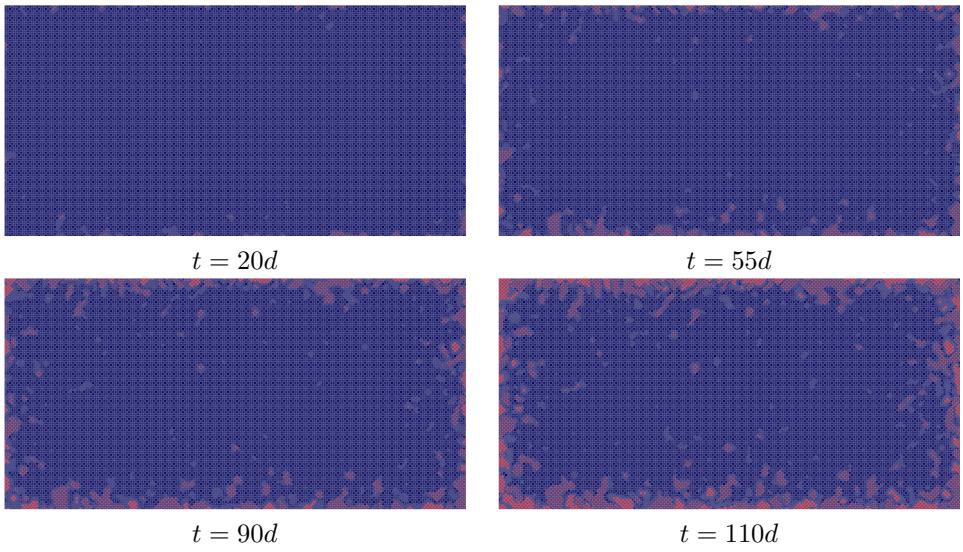

FIG. 6.2. *Time evolution of the chalcopyrite phase with small stochastic Fokker-Planck term in f_l. At $t = 0d$ only sphalerite (blue) is present (not displayed). As Cu enters from the boundary, chalcopyrite (red) forms. One can observe that the segregation starts with small islands that grow steadily.*

Due to the boundary conditions, the Cu concentration increases in Ω during the computation. Once it exceeds a certain threshold, as a consequence of the free energy minimisation (2.7), chalcopyrite (in red) is formed. The graph of Zn behaves opposite to that of Cu. The concentration of Fe is not displayed, it is a perfect constant in time and space.

As the experimental pictures of chalcopyrite disease within sphalerite suggest, there is a competition between elastic energy and surface energy. Yet, there is a mechanism missing that destroys the symmetry. Subsequently we assume that local changes arise in the free energy densities. These changes may be due to inhomogeneities of the material, and impurities in turn can be the seed for nucleation of chalcopyrite.

A stochastic source term in the context of spinodal decomposition has first been introduced by Cook, [7]. Langer [13] has developed a statistical theory of spinodal decomposition leading to a Fokker-Planck equation. The stochastic source ξ is a white noise term and is added to the free energies f_l by setting

$$f_1(c) = f^1(c) + \xi(x,t), \qquad f_2(c) = f^2(c) - \xi(x,t), \tag{6.1}$$

where again $f^l(c)$ denote the tabulated energies of the harmonic approximation. FIG. 6.2 visualizes the result of the computations with the stochastically disturbed free energy. We see that the solution looks very similar to the in-situ observations and also predicts small chalcopyrite islands that proceed the main segregation front.

Acknowledgments. The author thanks the German Research Community DFG for the financial support within the priority program 1095 *Analysis, Modeling and Simulation of Multiscale Problems.*

REFERENCES

[1] N. M. Ashcroft and N. D. Mermin, *Solid State Physics*, Saunders College Pub., 1976.
[2] K. Bente and T. Doering, Eur. J. Mineral. **10** (1993), 465.
[3] K. Bente and T. Doering, Min. Petrol. **53** (1995), 285–305.
[4] T. Blesgen, S. Luckhaus and K. Bente, *Modeling and Numerical Simulation of Diffusion Induced Segregation*, Cryst. Res. Tech. **37** (2002), 570–580.
[5] T. Blesgen, *A Revised Model for Diffusion Induced Segregation Processes*, J. Math. Phys. (2005), DOI 10.1063/1.1840292.
[6] T. Blesgen, S. Luckhaus and K. Bente, *Diffusion Induced Segregation in the Case of the Ternary System Sphalerite, Chalcopyrite and Cubanite*, Cryst. Res. Tech. **39**, 969–979.
[7] H. E. Cook, Acta Metall. **18** (1970), 297–306.
[8] M. T. Dove, *Introduction to Lattice Dynamics*, Cambridge University Text, 1993.
[9] J. D. Gale, *GULP-A Computer program for the symmetry adapted simulation of solids*, JCS Faraday Trans. **93** (1997), 629.
[10] X. Gonze, J.-M. Beuken, R. Caracas, F. Detraux, M. Fuchs, G.-M. Rignanese, L. Sindic, M. Verstraete, G. Zerah, F. Jollet, F. Torrent, A. Roy, M. Mikami, P. Ghosez, J.-Y. Raty, D. C. Allan, *First-principles computation of material properties: the ABINIT software project*, Comput. Mat. Science **25** (2002), 478–492.
[11] P. Hohenberg and W. Kohn, Phys. Rev. B **136** (1964), 136.
[12] W. Kohn and L. J. Sham, *Self-Consistent Equations Including Exchange and Correlation Effects*, Phys. Rev. A **140** (1965), 1133.
[13] J. S. Langer, Ann. Phys. **65** (1975), 53-86.
[14] E. H. Nickel, Information Circular IC 170 Department of Mines, Technical Surveys, Ottawa, 1965.
[15] L. Onsager, *Reciprocal relations in irreversible processes I*, Phys. Rev. **37** (1931), 405–426.
[16] M. C. Payne, M. P. Teter, D. A. Allan, T. A. Arias and J. D. Joannopoulos, *Iterative minimization techniques for ab initio total-energy*, Rev. Mod. Phys. **64** (1992), 1045–1097.
[17] N. Troullier and J. L. Martins, Phys. Rev. B **43** (1993), p. 1991.